Published online 2 July 2020

Nucleic Acids Research, 2020, Vol. 48, No. 16 ***e91***
doi: 10.1093/nar/gkaa550

A fully-automated method discovers loss of mouse-lethal and human-monogenic disease genes in 58 mammals

Yatish Turakhia[1,†], Heidi I. Chen [2,†], Amir Marcovitz[2,†] and Gill Bejerano [2,3,4,5,*]

[1]Department of Electrical Engineering, Stanford University, Stanford, CA 94305, USA, [2]Department of Developmental Biology, Stanford University, Stanford, CA 94305, USA, [3]Department of Computer Science, Stanford University, Stanford, CA 94305, USA, [4]Department of Biomedical Data Science, Stanford University, Stanford, CA 94305, USA and [5]Department of Pediatrics, Stanford University, Stanford, CA 94305, USA

Received January 23, 2020; Revised May 23, 2020; Editorial Decision June 16, 2020; Accepted June 23, 2020

ABSTRACT

Gene losses provide an insightful route for studying the morphological and physiological adaptations of species, but their discovery is challenging. Existing genome annotation tools focus on annotating intact genes and do not attempt to distinguish nonfunctional genes from genes missing annotation due to sequencing and assembly artifacts. Previous attempts to annotate gene losses have required significant manual curation, which hampers their scalability for the ever-increasing deluge of newly sequenced genomes. Using extreme sequence erosion (amino acid deletions and substitutions) and sister species support as an unambiguous signature of loss, we developed an automated approach for detecting high-confidence gene loss events across a species tree. Our approach relies solely on gene annotation in a single reference genome, raw assemblies for the remaining species to analyze, and the associated phylogenetic tree for all organisms involved. Using human as reference, we discovered over 400 unique human ortholog erosion events across 58 mammals. This includes dozens of clade-specific losses of genes that result in early mouse lethality or are associated with severe human congenital diseases. Our discoveries yield intriguing potential for translational medical genetics and evolutionary biology, and our approach is readily applicable to large-scale genome sequencing efforts across the tree of life.

INTRODUCTION

The placental mammal radiation exhibits tremendous phenotypic diversity (1). This myriad form and function arose from gain, loss, and modification of inherited traits from one generation to the next. Genomic sequence comparisons reveal that, similarly, genes arose, were modified, and died through evolutionary time across different lineages. While it is nearly impossible to be certain that a gene locus no longer emits any kind of coding or non-coding transcript, ancestral ‘gene loss’ by virtue of losing or dramatically altering coding potential is well-established (2) and could contribute to the sequence basis of phenotypic evolution.

Previous studies have identified a few intriguing examples of gene losses that are associated with phenotypic traits. For example, the enzyme gene *GULO* is inactivated in independent mammalian lineages that likely consequently lost the ability to synthesize Vitamin C, which must instead be constantly supplied by their diet (3,4); multiple visual system genes are no longer functional in subterranean mammals which live primarily in darkness (5,6); taste receptor and other genes are lost in fully aquatic cetaceans (7–9); renal transporter genes *URAT1*, *GLUT9* and *OAT1* are dead in fruit-eating bats, which could have facilitated their frugivorous diet (10); the immune genes *MX1* and *MX2* are eroded in toothed whales, possibly making them more susceptible to certain viral pathogens (11); and the loss of *PON1* in several marine mammals may increase their vulnerability to agricultural pesticide pollution (12). Systematic annotation of gene losses across species could, therefore, not only reveal fascinating evolutionary events and genotype-phenotype relationships, but could also highlight ‘natural knockout’ models for human pathologies that point to compensating molecular pathways in species missing otherwise-indispensable genes (2,3,13).

[*]To whom correspondence should be addressed. Tel: +1 650 725 6792; Email: bejerano@stanford.edu
[†]The authors wish it to be known that, in their opinion, the first three authors should be regarded as Joint First Authors.
Present address: Yatish Turakhia, Genomics Institute, University of California, Santa Cruz, CA 95064, USA.

Manual annotation, such as ENCODE-HAVANA (14), is the gold standard for labeling pseudogenized genes but has only been applied to a handful of species (human, mouse, rat, and zebrafish) and is not scalable for hundreds to thousands of newly sequenced species (15). Automating the discovery of gene losses is scalable but challenging. For example, Sharma *et al.* (10) recently attempted an automated method using whole-genome multiple-sequence alignment to identify genes with inactivating mutations. However, their overly inclusive approach reportedly predicted hundreds of gene losses per species across 62 mammals, of which only 21 losses in total are discussed in the paper, presumably because manual inspection deemed many loss predictions inconclusive at best. A similar technique was used to further semi-manually annotate 85 gene losses in cetaceans (16). Other computational approaches for gene annotation, like the Ensembl pipeline (17), combine *ab initio* predictions with protein sequence evidence (18) and with gene models inferred from RNA-seq data. However, they focus only on annotating *intact* genes and do not attempt to distinguish decaying genes from those that only confoundingly appear so in regions of low sequence coverage, poor sequence quality, or dubious alignment calls. A clear need exists for a method that automatically calls gene losses with high confidence.

We developed a novel, conservative approach for identifying gene loss events and applied it to 58 mammalian genomes, using human assembly hg38 as the reference. We hypothesized that the most effective strategy for declaring loss of an ancestral gene function is to demonstrate that it is highly sequence-eroded compared to other genes in the same genome. While it is impossible to guarantee that no gene transcript is expressed from the orthologous locus (especially if a known promoter remains intact), the erosion of gene sequence implies that the gene does not maintain its original function.

To that end, we used pairwise whole-genome alignments to locate the orthologs of human protein-coding genes in each of the 58 query species by applying a novel synteny-aware mapping procedure. We employed a Mahalanobis distance-based model to identify the most highly mutated orthologs in each genome in a way that normalizes for the baseline extent of sequence divergence between this species and the reference (human). We considered these per-genome predictions to be *likely eroded* and functionally altered orthologs in the sequenced individual, and thus possibly the species represented by the assembly. Lastly, we applied a stringent phylogenetic filter, requiring that all final candidate erosions were supported by observations from at least two closely related species and affected ancestral genes—in order to minimize confounders due to assembly artifacts, private (individual-specific) mutations, or reference genome biases. Though very conservative, our approach uncovered hundreds of *high-confidence ortholog erosion* (*hcoErosion*) events, affecting over 50 mammals, including some very surprising gene losses with intriguing evolutionary and biomedical implications. Importantly, our method was designed to allow easy addition of genomes to the analysis, such as the those from countless newly sequenced mammals, birds (19), vertebrates (20), insects (21), etc.

MATERIALS AND METHODS

Genome assemblies, reference genome and protein-coding gene annotations

We used genome assemblies of 59 mammalian species (listed in Supplementary Table S1) in this study, with human genome assembly GRCh38/hg38 as reference. From Ensembl biomart release 86, we downloaded lists of gene identifiers and counted how many unique 'protein_coding' gene identifiers are found. Of the 59 aligned mammalian species, 34 species had gene annotation in Ensembl. For our reference gene set, we started with 22 072 unique human protein-coding genes annotated in Ensembl and excluded gene annotations from un-placed and un-localized scaffolds, leaving 19 729 protein-coding genes. We then obtained coordinates for segmental duplications (genomic fragments larger than 1 kb with >90% sequence identity to other genomic fragments) from the UCSC genome browser and excluded from our analysis genes with 10% or more overlap with any segmentally duplicated fragment. We also restricted the reference gene set to genes having 'complete' Ensembl transcripts. These filters generated our reference gene set of 17 860 unique human protein-coding genes for mapping across mammalian genomes. We collected assembly N50 measures for each genome from NCBI: https://www.ncbi.nlm.nih.gov/assembly.

Mapping orthologs across mammalian genomes

We used Jim Kent's BLASTZ-based, whole-genome pairwise alignment chains (22) to map—when possible with high confidence—each reference gene to a single orthologous position in each of the 58 query species (Figure 1A). First, we assigned every exonic (CDS+UTR) base in the canonical transcript of the reference gene to the highest-scoring chain (in terms of UCSC chain alignment scores) that contains the base in its alignment (Figure 1B1– B2). The chain to which most number of exonic bases get assigned was picked as the *best chain* (C_b) for that gene (Figure 1B3). Since chains are preferentially ordered based on the alignment score before assigning exonic bases (Figure 1B1), the best chain was also the chain with highest conservation of synteny for those aligning bases, and was treated as the most likely ortholog for that gene. Next, this procedure was repeated after removing the *best chain* (C_b) from consideration to pick another chain as the *second-best chain* (C_{sb}) for the same gene (Figure 1B4). This chain C_{sb} was treated as containing a likely paralog of the gene. To ensure that the orthologous chain was easily differentiable from paralogs, we required the *second-best chain* to have an alignment score at least 20 times lower than that of the best chain. To also ensure high conservation of synteny , we required the number of bases in the aligning blocks of the best chain be at least 20 times greater than the number of bases in the gene itself—i.e. *gene-in-synteny* $\geq$ 20, where *gene-in-synteny* = length of C_{b}/length of gene. We also required unique mapping of coordinates between reference and query genomes, such that if two or more reference genes were mapped to the same query location, all overlapping mappings were discarded.

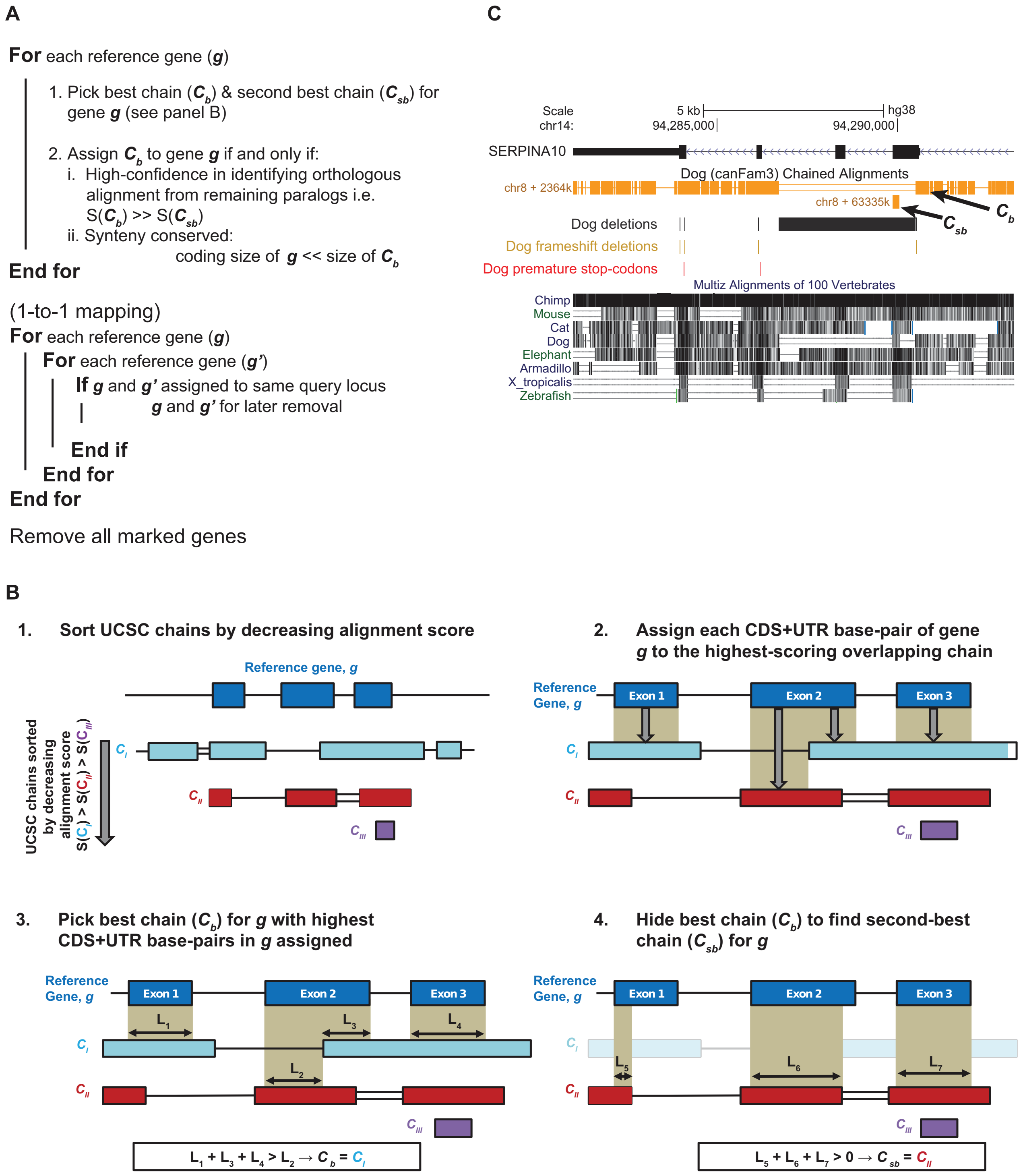

```
For each reference gene ($g$)
    1. Pick best chain ($C_b$) & second best chain ($C_{sb}$) for
       gene $g$ (see panel B)

    2. Assign $C_b$ to gene $g$ if and only if:
       i. High-confidence in identifying orthologous
          alignment from remaining paralogs i.e.
          $S(C_b) >> S(C_{sb})$
       ii. Synteny conserved:
                    coding size of $g$ << size of $C_b$
End for

(1-to-1 mapping)
For each reference gene ($g$)
    For each reference gene ($g'$)
        If $g$ and $g'$ assigned to same query locus
            $g$ and $g'$ for later removal

        End if
    End for
End for

Remove all marked genes
```

A
C
B
1. Sort UCSC chains by decreasing alignment score
Reference gene, g
UCSC chains sorted by decreasing alignment score S(C_I) > S(C_II) > S(C_III)
C_I
C_II
C_III
2. Assign each CDS+UTR base-pair of gene g to the highest-scoring overlapping chain
Reference Gene, g
Exon 1
Exon 2
Exon 3
C_I
C_II
C_III
3. Pick best chain (C_b) for g with highest CDS+UTR base-pairs in g assigned
Reference Gene, g
Exon 1
Exon 2
Exon 3
L1
L2
L3
L4
C_I
C_II
C_III
L1 + L3 + L4 > L2 → C_b = C_I
4. Hide best chain (C_b) to find second-best chain (C_sb) for g
Reference Gene, g
Exon 1
Exon 2
Exon 3
L5
L6
L7
C_I
C_II
C_III
L5 + L6 + L7 > 0 → C_sb = C_II
Scale
chr14:
5 kb
hg38
94,285,000
94,290,000
SERPINA10
Dog (canFam3) Chained Alignments
chr8 + 2364k
chr8 + 63335k
C_b
C_sb
Dog deletions
Dog frameshift deletions
Dog premature stop-codons
Multiz Alignments of 100 Vertebrates
Chimp
Mouse
Cat
Dog
Elephant
Armadillo
X_tropicalis
Zebrafish

Figure 1. Chain-picking method to map genes from a reference genome to an orthologous locus in query species genome. (**A**) We designed a conservative gene-by-gene scanning approach that maps genes from a reference genome (here human, GRCh38) to their orthologous locations in target mammalian genomes based on pairwise genome chain alignments. For each reference gene, our approach first picks two chains: the *best chain* (C_b) and the *second-best chain*, C_{sb} (panel B). The chain C_b is then assigned to a gene g if (i) it has a significantly better alignment score relative to the other chain C_{sb} so that the orthologous region can be unambiguously distinguished from remaining paralogs, (ii) it is much larger than the coding size of g such that it ensures sufficient conservation of synteny for the flanking genomic context, and (iii) it maps g to a locus in the target genome that no other gene g' is mapped to, so as to ensure 1-to-1 mapping of genes to query locus. (**B**) Detailed illustration of the procedure to pick the *best-chain* (C_b) and the *second-best chain* (C_{sb}) for gene g. In the case of multiple chains at a locus (gene, g), our procedure first assigns each exonic (CDS+UTR) base of g to the highest-scoring chain overlapping with the base-pair, and then identifies the chain (C_b) to which the most exonic bases of g were assigned. The procedure is repeated to identify another chain (C_{sb}) after C_b is hidden. (**C**) *SERPINA10* is a known loss of function gene in dogs (34), and hence lacks any annotations or orthology mapping from human to dog. This pairwise, chain-based approach enables precise mapping of an intact gene from a reference assembly to sequence-eroded loci in another species.

In each species, for every gene to which an orthologous chain was assigned, we used the alignments derived from the chain to determine the orthologous amino acid sequence for every transcript of that gene. Because exon boundaries sometimes shift for evolutionary or alignment reasons, we excluded the first and last two amino acid positions in each exon for all downstream analyses (23). Gaps in chain alignments found in regions containing an assembly gap in the query species were masked out to avoid confusing them with true deletions in the query genome. Note that, while UCSC genome browser views of multiple sequence alignments are shown for compact visualization in the Results section, only pairwise alignments were used for the underlying computation described here.

Outlier detection model

To identify the genes orthologs that have a surprisingly high number of amino acid substitutions and deletions in each of the 58 query species, we used an outlier detection approach. We first used the derived amino acid sequence of each transcript for every gene in a query species, as described above, to compute a feature vector $\vec{x} = (x_1, x_2)$, where x_1 is the fraction of the transcript amino acids deleted in the query species and x_2 is the fraction of non-synonymous amino acid substituted in the remaining portion of the gene transcript compared to the orthologous gene transcript sequence in the reference species (human).

We then used $\vec{x}$ across all genes in the query species to compute the mean vector, $\vec{\mu}$, and a covariance matrix, S. Mahalanobis distance (MD) (24,25) measures how 'far' a given gene with feature vector, $\vec{x}$, is from the distribution of all genes in the query species, as follows:

$$\mathrm{MD} = \sqrt{(\vec{x} - \vec{\mu})^{\top} S^{-1} (\vec{x} - \vec{\mu})} \qquad (1)$$

Since most genes exhibit relatively few non-synonymous substitutions and deletions (as placental mammals are relatively closely related, see Figure 2B), a large value of MD implies extensive erosion of the gene. Conversely, a small value of MD implies that the gene is well-conserved. Since the coding sequences are expected to diverge more with increasing phylogenetic distance between reference and query species, we computed a different distribution ($\vec{\mu}$ and S) for each query species. If all transcripts of an ortholog had MD greater than an absolute threshold ($\mathrm{MD} > 15$), we marked the gene an outlier (✗) since it is likely sequence-eroded and nonfunctional in the species represented by the query genome. If all transcripts of an ortholog exhibited $\mathrm{MD} \leq 5$, we regarded the gene sequence-conserved and functional (✓) in the species represented by the query genome. All other orthologs that were not categorized into either of the former two groups were marked with undetermined (?, see Figure 2C).

Phylogenetic filtering

We used the phylogenetic tree of the 59 mammalian species (including human; Supplementary Figure S1) to identify which of the outlier orthologs would be considered to have undergone hcoErosion (Figure 2D illustrates this procedure). For each gene, we recorded which species exhibit a sequence-conserved ortholog (based on the results of the outlier detection model described above; also see Figure 2B, C). Since the gene under consideration is already annotated to be functionally present in hg38 by Ensembl, we inferred by parsimony that the last common ancestor of human and of all species containing the conserved gene likely had a functional copy of this gene with a sequence similar to that of its extant functional orthologs. Finally, we search all subtrees starting from the earliest ancestral species marked in this fashion with gene conservation to identify specific groups where hcoErosion has occurred. A group in which hcoErosion has occurred (Figure 2D) is one in which there are at least two species with the gene marked as likely eroded (all transcripts with $\mathrm{MD} > 15$) and no leaf-node species with the gene marked as sequence-conserved ($\mathrm{MD} \leq 5$).

Curation of UniProt data and details of FPR (False Positive Rate) estimation in mouse and rat

To measure the rate of false positives in hcoErosion predictions for mouse and rat, we obtained experimentally curated coding gene models downloaded as protein sequences with 'protein level' or 'transcript level' evidence from UniProt (18) (release-17_01; ftp://ftp.uniprot.org/pub/databases/uniprot/current_release/knowledgebase/complete). We found 16 385 and 7591 gene models in mouse and rat, respectively. We then mapped those amino acid sequences to their respective genomes (mouse sequences to mm10; rat sequences to rn6) using protein BLAT (26) with default settings (minimum mapping score 30; minimum sequence identity 25; maximum intron size 750 000). After mapping these protein sequences, we computed what proportion of orthologs predicted to be affected by hcoErosion is contradicted by empirical evidence. Specifically, for a given species and its genome, any predicted hcoErosion-affected orthologs that deviate by >20% in sequence length, share <90% identity, or disagree with the locus of the relevant UniProt sequence were considered false predictions. Lastly, since we had 17 860 tested proteins in the reference gene set, we conservatively scaled up the number of conflicts in mouse and rat by a factor of 1.09 (=17 860/16 385) and 2.35 (=17 860/7591), respectively, to estimate our false positive rate (FPR) while accounting for potentially missing UniProt entries.

Curation of lethal loss-of-function genes in mouse models

We used gene function annotations from the MGI Phenotype Ontology (Mouse Genome Informatics, http://www.informatics.jax.org/) to derive a subset of genes whose disruption leads to severe developmental perturbations and lethal consequences (27). The MGI Phenotype Ontology catalogs spontaneous, induced, and genetically-engineered mouse mutations and their associated phenotypes. Ontology data (containing 8949 phenotypic terms; v6.04) were lifted over from mouse to human, resulting in 609 253 (canonicalized) gene-phenotype associations. We selected all 50 unique phenotypic terms (Supplementary Table S2) with the string 'lethal' in their description (e.g., MP:0008762 *embryonic lethality*; MP:0008569 *lethality at*

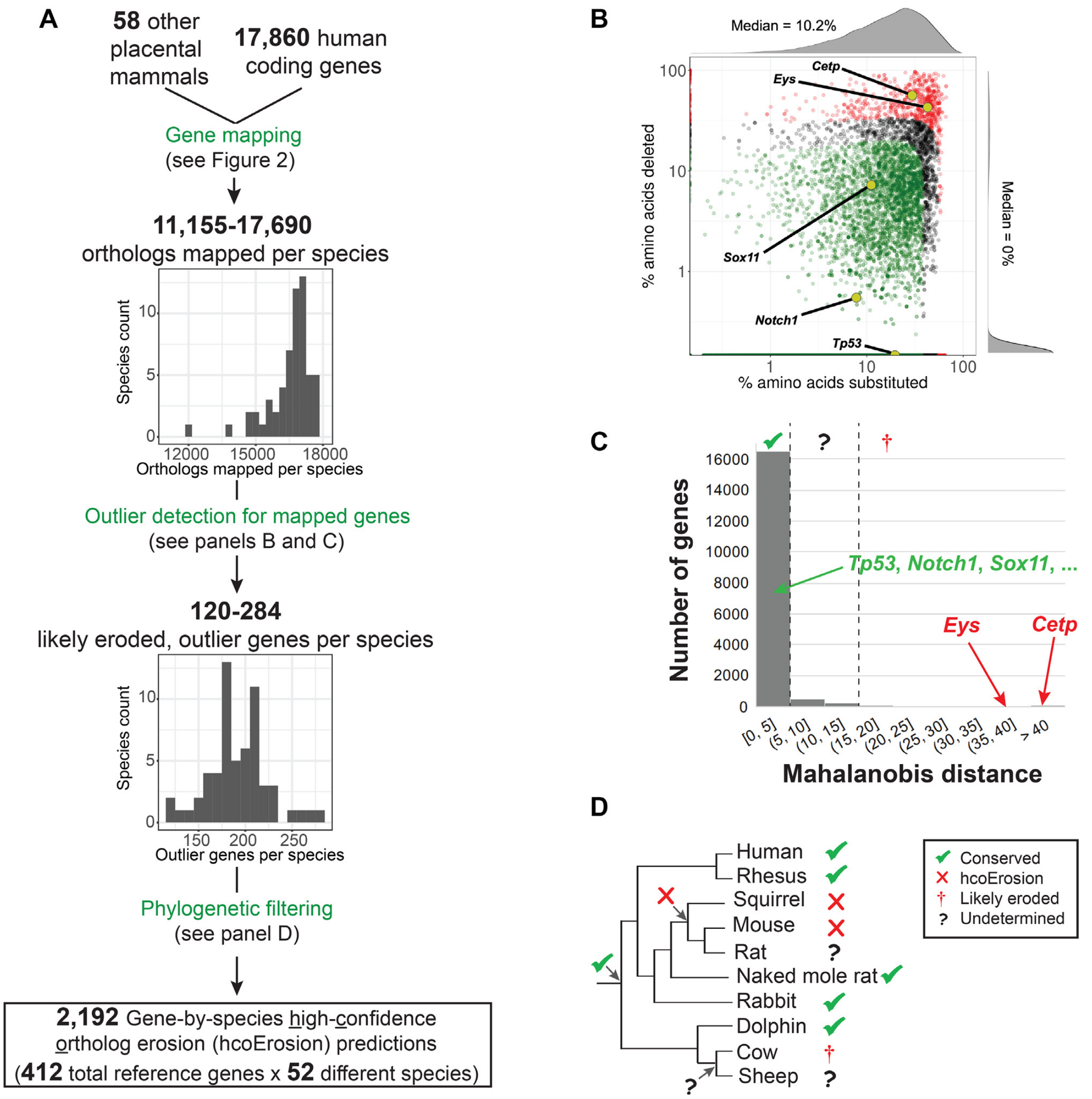

Figure 2. A pipeline to call hcoErosions. (**A**) Using pairwise chained alignments, we determined an orthologous location for human coding genes in each genome (Figure 1). Then we computed the amount of amino acid deletion and substitution to find, for each each genome, the outlier genes among all the genes that were mapped (i.e., likely eroding genes). (**B**) Scatter plot showing the distribution of the mouse (mm10) genes along the two features (*% amino acids substituted* and *% amino acids deleted*) for calculating Mahalanobis Distance (*MD*). The histogram along each axis shows the distribution of points when projected on the respective axis; for example, the peak in the histogram parallel to the y-axis illustrates a high density of overlapping points abutting the x-axis. Per-species likely eroded genes (in red, such as known losses of *Cetp* and *Eys*) have much higher values of *% amino acids substituted* and *% amino acids deleted* compared to intact (in green) and undetermined genes (in black). (**C**) Histogram of the *MD* values for mouse genes along with the threshold values (dashed vertical lines) for conserved (✓, $MD \leq 5$), undetermined (?), and likely eroded (†, $MD > 15$) genes. (**D**) An example illustration of applying phylognetic filtering. We call hcoErosion (×, e.g. in mouse and squirrel) if a gene is marked likely eroded ($MD > 15$) in more than one species in a clade that is flanked by at least one group in which the gene is conserved (✓). An undetermined gene in an individual species (?, e.g. in rat) is inferred as eroded if it resides in a clade with hcoErosion. The likely eroded (†) gene in cow, however, is not considered a hcoErosion since the finding is not supported by another adjacent species.

weaning; MP:0006206 *embryonic lethality between somite formation and embryo turning*), identifying a total of 3617 genes associated with causing early lethality when disrupted.

Analysis of hcoErosion genes implicated in HGMD

The professional version (16.2) of the Human Gene Mutation Database (28) contains 165 939 entries of known disease-causing gene mutations (referenced to GRCh38 assembly) and their respective phenotypes. We obtained the list of 4014 monogenic disease genes (i.e. genes with at least one 'DM' mutation) from this database, of which 3711 genes were also present in our reference gene set.

Analysis of genic variation intolerance with RVIS and pLI scores

Residual Variation Intolerance Score (RVIS) is a unified genome-wide metric that quantifies the extent to which genes tolerate coding mutation load (i.e. the higher the score, the more a gene can tolerate common genetic variation without negative consequences) (29). We used the pre-computed RVIS percentiles based on Exome Aggregation Consortium variants with Minor Allele Frequency $\geq 0.05\%$ (http://genic-intolerance.org/data/RVIS_Unpublished_ExACv2_March2017.txt) to identify hcoErosion genes with scores in the bottom quintile likely to be intolerant to functional variation in humans. We performed a two-tailed Mann–Whitney U test to assess whether there is a significant difference between the RVIS percentile distribution of hcoErosions compared to the reference gene set. We also screened for any additional hcoErosion genes that have a high probability of being loss-of-function intolerant (pLI) score of $\geq$0.9 using publicly available data (https://storage.googleapis.com/gnomad-public/release/2.1.1/constraint/gnomad.v2.1.1.lof_metrics.by_gene.txt.bgz); we used the threshold of $\geq$0.9 per the convention established by pLI score developers Lek *et al.* for flagging genes that are very likely intolerant to functional variation (30).

Statistical significance of depletion

To estimate statistical significance of depletion (31) for the hcoErosion group of genes relative to categories such as mouse lethal genes or HGMD disease genes or genes with pLI $\geq$0.9, we used the Fisher exact test to compute a one-sided P-value:

$$p_{\text{depletion}} = \binom{\Pi}{L_\Pi}\binom{N-\Pi}{L-L_\Pi}/\binom{N}{L} \qquad (2)$$

In the above equation, N and L denote the total number of genes and the hcoErosion subset of genes in the analysis, respectively. Similarly, Π and L_Π denotes the subset of N and L associated with a gene category such as HGMD disease genes or mouse lethal genes.

We also compute a 'fold change' for depletion as $1/\text{Fold}_{\text{enrichment}}$:

$$\text{Fold}_{\text{depletion}} = \frac{1}{\text{Fold}_{\text{enrichment}}} = \frac{\Pi * L}{N * L_\Pi} \qquad (3)$$

Tissue and pathway enrichment of hcoErosion genes

To determine if expression of the 412 unique hcoErosion genes might be enriched in particular tissues, we used the TissueEnrich tool (32), providing the hcoErosion gene names as input. To determine if the 412 unique hcoErosions are enriched in biological functions and/or compartments, we used the GREAT v4.0.4 tool (33), providing the Ensembl 86 human canonical transcription start sites as input, considering terms annotating $\geq$30 and $\leq$1000 genes, and using the 'basal plus extension' association rule. We report all tested ontology terms with a hypergeometric FDR Q-value $<$0.05 and fold enrichment $\geq$2.

RESULTS

Pre-existing gene annotation methods fail to identify and determine the functional state for thousands of orthologs

Of the 59 mammalian genomes (including the human reference) that we used in our study, Ensembl gene predictions (release 86) were available for 34 genomes. The number of protein-coding gene annotations varied widely (Figure 3A), from 11 765 annotations in alpaca to 22 285 annotations in human. When plotting the number of Ensembl predicted genes against the assembly N50, it is clear that the annotation completeness is artifactually dependent on the level of assembly contiguity (Figure 3A). For instance, absence of the critical chordate development gene *PAX6* in the dog annotation set is likely due to a sequencing gap in the genome assembly (Figure 3B). Similarly, while *TP53* and multiple adjacent genes are absent from the alpaca annotation set, its genome includes a region with high sequence similarity to the human *TP53* ortholog (Figure 3C), implying a potentially missed prediction. Labour-intensive, manual pseudogene annotation pipelines are similarly incomplete, tackling a handful of species and still working on key species pseudogene sets (https://www.gencodegenes.org/). Based on these observations, we devised an improved approach for identifying a high-confidence, conservative subset of gene loss events across the 58 placental mammals, using human as the reference.

Mapping gene orthologs across mammalian genomes

To identify *ab initio* orthologs of human genes across the 58 query species, we used whole-genome pairwise alignments (i.e. Jim Kent's BLASTZ-based *chains* (22)) to map genes from human coordinate space to each of the other genomes. Chains identify conserved sequences not only in coding regions (covering 2% of the human genome) but also in non-coding, gene-regulatory regions (covering 5–10% of the human genome) in which the genes are interspersed. As such, chains facilitate accurately determining genomic orthology between species. Using these 58 pairwise alignment chains anchored to the human reference, we determined the single locus in the aligning (query) genome that exhibited the greatest sequence similarity and conservation of synteny with each human protein-coding gene. Specifically, each successfully mapped gene was (i) positioned within a chain that had alignment and gene-in-synteny scores sufficiently higher than the next-highest-scoring (likely paralogous) chain and (ii) did not overlap in genomic space with any other gene mappings proposed in the previous step (see Materials and Methods, Figure 1A, B). In total, our mapping procedure identified 11 155–17 690 orthologs per species (median: 16 782; Figure 2A) across the 58 non-human mammals considered.

Importantly, this chain-based mapping approach worked correctly for previously known gene losses, accurately identifying pseudogenized orthologs with extensive sequence erosion compared to the ancestral gene. For example, much of the exonic portions of *SERPINA10* are absent in the dog genome and do not yield a functional gene product (34). As such, Ensembl does not offer a corresponding gene annotation in the dog genome assembly (canFam3), which would leave ambiguity about the existence and function this ortholog in dogs if not for experimental evidence. Our approach, however, precisely located the remnants of *SERPINA10* in the canFam3 assembly and allowed for assessing the semantic status (reading frame integrity and occur-

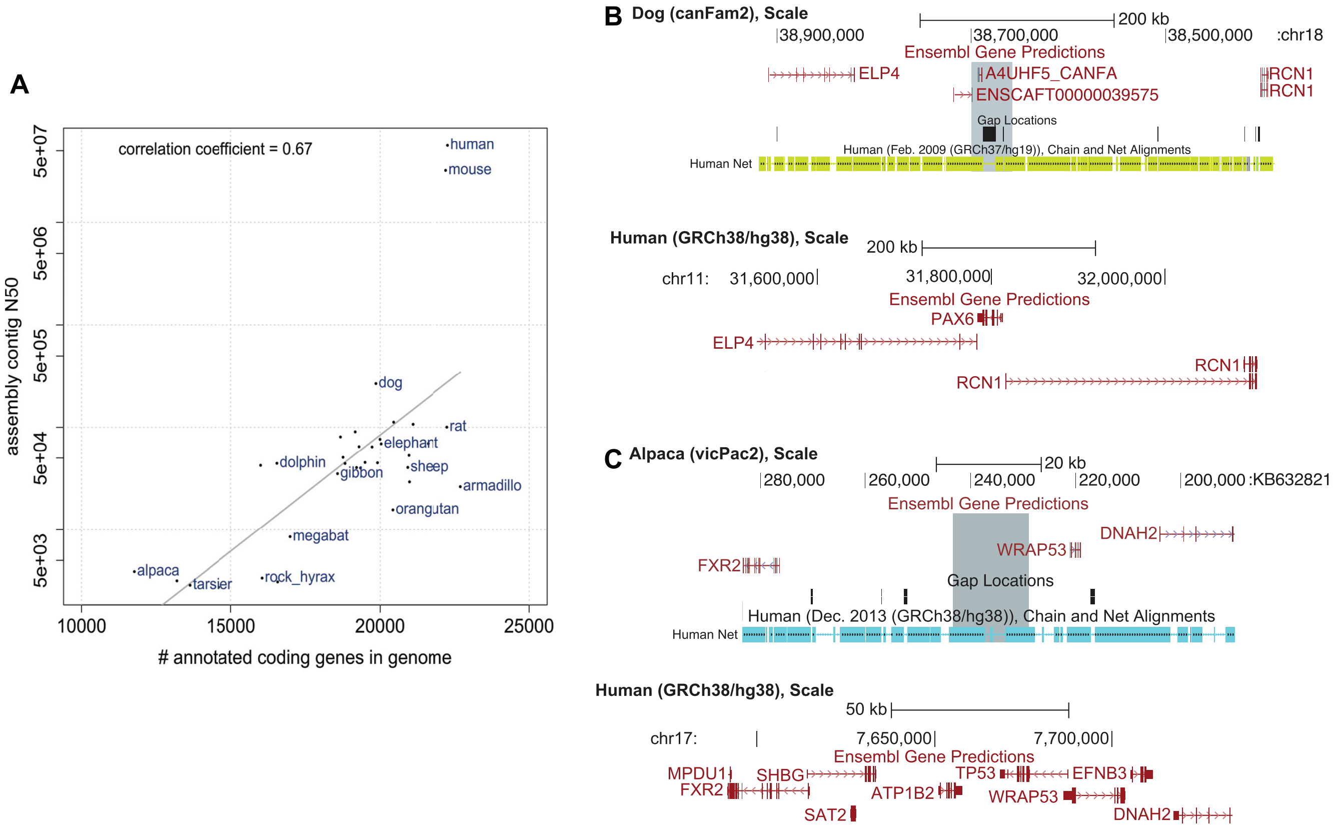

Figure 3. Incomplete coding gene annotations in genomic databases. (**A**) Of the 59 mammalian genomes used in this study, 34 have Ensembl (release 86) gene annotations. The number of gene annotations per genome correlates with assembly quality (as measured by N50 contig length), suggesting that gene loss should not be inferred from a missing ENSEMBL ortholog in a lower N50 genome. (**B**) Top: *pax6* Ensembl gene model artefactual absence (gray highlight) in the dog genome assembly due to a sequencing gap. The genome browser view shows the minus strand. Bottom: The orthologous position of *PAX6* (and flanking genes) in the human genome. (**C**) Top: *TP53* Ensembl gene model absence (gray highlight) in the alpaca genome within a conserved region.The genome browser view shows the minus strand. Bottom: The orthologous position of *TP53* (and flanking genes) in the human genome.

rence of substitution, insertion, and deletion) of the remaining chain-mapped exons (Figure 1C).

Per-species identification of likely eroded orthologs using a Mahalanobis distance outlier model

Because functional gene inactivation will be accompanied by relaxation of purifying selection on all genomic regions encoding the gene, we used the extent of coding sequence erosion to declare the loss of gene function. In particular, to account for mutation rate heterogeneity across different branches of the mammalian tree, we restricted our results to orthologs that appear extremely eroded (using outlier detection) in sequence *relative* to all other mapped genes in the same given species. Unlike Sharma *et al.* (10), who used single-event features, such as in-frame stop codons and frameshift indels, we considered two different aggregate features of sequence erosion—i.e. the fraction of amino acids affected by substitutions and the fraction of exonic amino acids out-right deleted with respect to the sequence of the human ortholog. This way, we avoided making spurious outlier calls caused by some mutations, such as stop codons near the end of a gene or multiple frameshift indels that restore the original frame, which do not necessarily lead to loss of the ortholog's function. Additionally, before declaring outliers, we masked out (i.e. did not consider) alignment gaps that could have resulted from sequencing gaps in the target species (see Materials and Methods).

For outlier detection, we used a Mahalanobis distance (*MD*) (24,25) based model (see Materials and Methods) to mark a small fraction of the orthologs (typically 1–2% or 120–284 genes per species, median of 192; Figure 2A) as outliers for their extreme fraction both of amino acid substitutions and deletions. We considered these outlier orthologs to be likely eroded in sequence and function in the species represented by the given genome assembly. For instance, by performing these methods on the 17 836 genes confidently mapped to the mm10 mouse assembly (Figure 2B), we correctly identified previously discovered gene losses for *Cetp* (35) and *Eys* (36) (plus other novel predictions) as outliers (MD $>$ 15), compared to uneroded, relatively sequence-conserved orthologs (MD $\leq$ 5), including genes *Tp53* (37), *Notch1* (38) and *Sox11* (39) (Figure 2B, C) with indispensable function in mice.

Phylogenetic filtering to identify high-confidence ortholog erosions in multiple related species

Two caveats must be considered for the per-species gene erosion predictions: Firstly, not all genes in the human reference set were necessarily present in functional form in the common ancestor shared by human and the species under

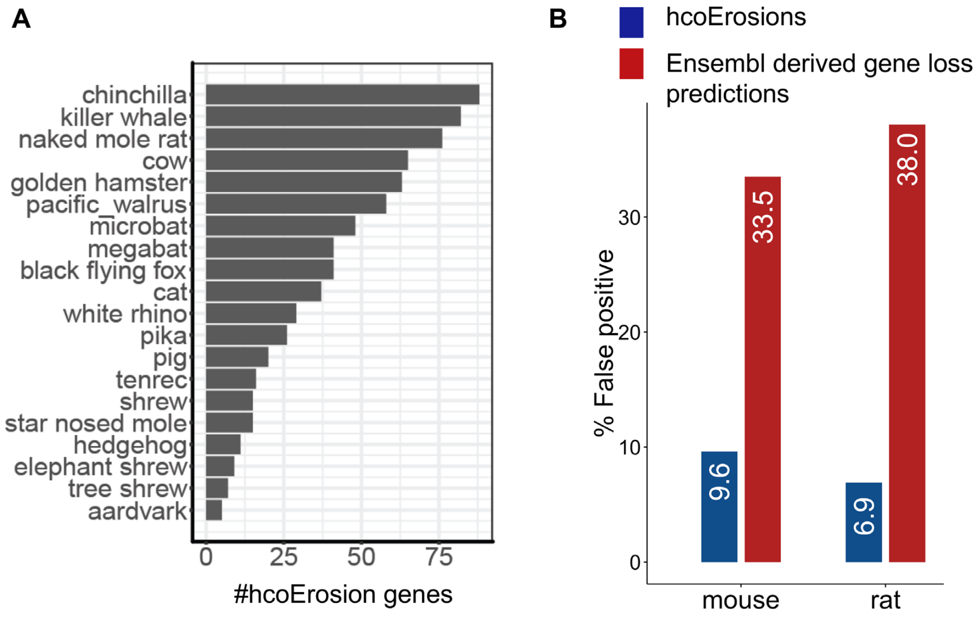

Figure 4. Distribution of hcoErosions across species and estimation of False Positive Rate (FPR). (**A**) Number of hcoErosions predicted in different species. (**B**) If hcoErosions are directly inferred by applying our phylogenetic filtering (Figure 2D) to missing gene annotations in Ensembl (instead of eroded genes from Figure 2C), the estimated FPR (red bars) in mouse and rat is significantly higher than in our set of predicted hcoErosions.

consideration. Sequences in other species that have some resemblance (such as paralogs) to a functional human gene, and that appear eroded, but were never present/functional in their common ancestor with human, could be confounded for gene erosion. Secondly, the erosion could be real but private to the single sequenced individual (i.e. not fixed in the species at-large).

To address these caveats, we applied strict phylogenetic filters to restrict the final candidate list to the highest-confidence predictions (Figure 2D). First, we required a final candidate to have an uneroded, sequence-conserved ortholog (MD $\leq$ 5) in at least one other mammal in addition to human such that the eroding species is internal to the subtree spanned by human and the other sequence conserving species. With the assumption of parsimony, this first step ensures that the candidate ortholog was present, of functional importance, and under purifying selection in the common ancestor of human and the eroding species. Second, even more importantly, we also required that each final candidate was considered likely eroded in *two or more* phylogenetically neighboring species (such as rat/mouse or manatee/elephant/cape elephant shrew) sharing a common ancestor with human in which the gene was declared conserved. Doing so minimized false positives from gene losses that are real but not fixed in a species, as well as those resulting from assembly, alignment, and mapping artifacts. We designated the final candidates as *high-confidence ortholog erosions* or *hcoErosions*.

In all, we identified 412 genes that were eroded in one or more multi-species groups , yielding 2192 and 539 unique gene-species and gene-clade pairs, respectively (Figure 2A, Supplementary Table S3). Our hcoErosion predictions include many previously known functional losses such as *Cetp* (35), *Eys* (36), and *Tcn1* (40) in mouse, *ZP1* in bovine genomes (41), *CRYGB* in subterranean mammals (5), *GSDMA* in whales (10), and *RHBG* in fruit bats (10). The number of hcoErosions per species ranged from 5 in aardvark to 88 in brush-tailed rat and chinchilla (median of 41, Figure 4A).

To estimate the false positive rate (FPR) for these results, we tabulated how many predicted hcoErosions for mouse and rat were contradicted by proteomic or even transcriptomic evidence from UniProt (18) (see Methods). We found 6/68 (8.82%) and 2/68 (2.94%) hcoErosion predictions in mouse and rat conflicting with UniProt evidence, respectively (Supplementary Table S4). We conservatively re-scaled the conflicts to account for potentially missing UniProt entries but still found the FPR estimate to be <10% in both species (Figure 4B, see Materials and Methods). In contrast, if we applied our phylogenetic filtering (Figure 2D) directly to the orthologs lacking Ensembl annotations for mouse and rat, the FPR for both species would be >30% (Figure 4B), highlighting the importance of our orthologous chain mapping and outlier detection approach.

Selection and variation in mammalian genes exhibiting multi-species ortholog erosion

We found that our final hcoErosion predictions (Supplementary Table S3), containing 412 unique human orthologs are depleted of genes causing lethality when inactivated in developing mice (*P*-value < 2.2e–16; fold = 8.43; Figure 5A), of known human HGMD disease-causing genes (*P*-value < 1.3e–11, fold = 3.17; Figure 5B), and of those with RVIS and pLI scores predicted to be intolerant to functional variation in humans (Figure 5C, *P*-value < 4.1e–24, fold = 19.94 and Figure 5D, *P*-value < 2.7e–35). Despite this depletion, 10 hcoErosions do involve genes whose knockout mouse models do not survive beyond early development (Table 1, see Methods). Likewise, 27 hcoErosions

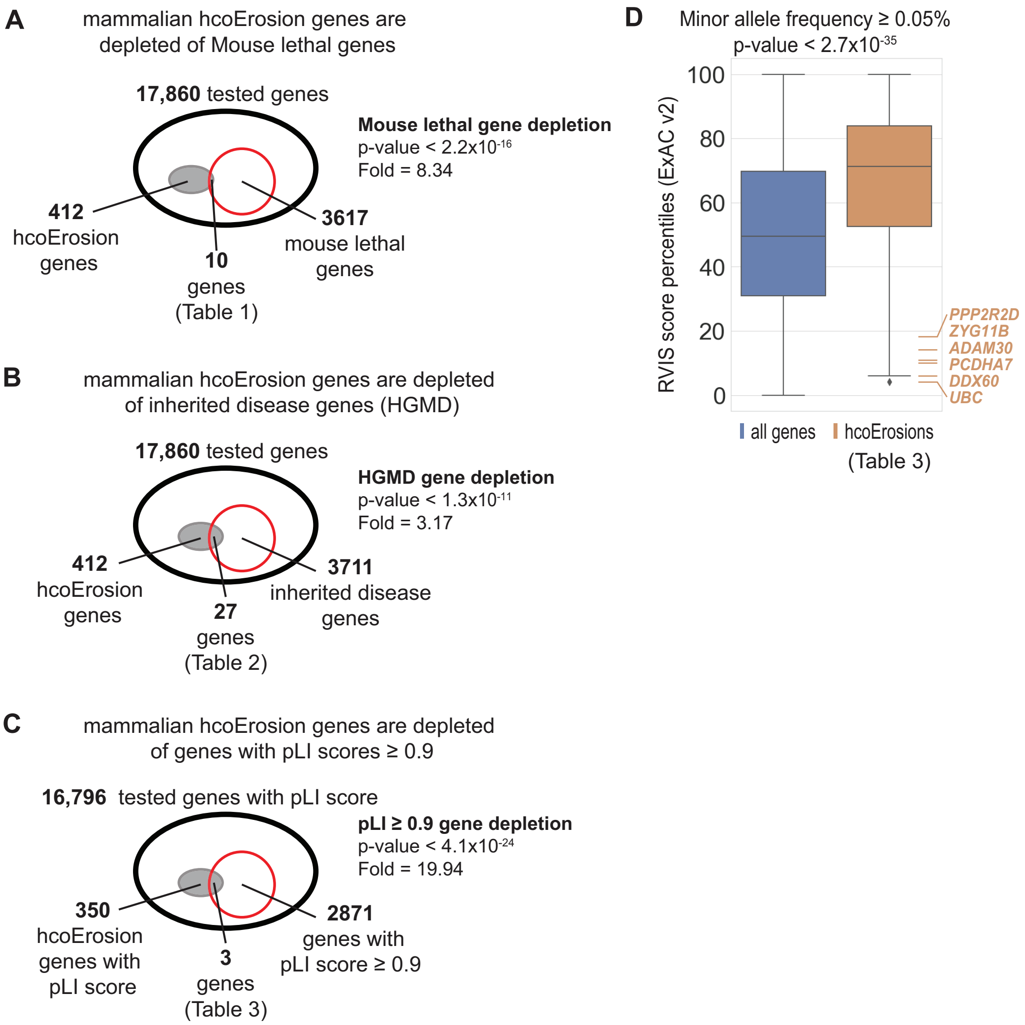

Figure 5. Selection and variation in mammalian genes affected by hcoErosion. hcoErosions are depleted of (**A**) genes whose inactivation in mouse models leads to lethality in early development; (**B**) genes with known Mendelian disease mutations (HGMD genes); and (**C**) genes with pLI scores ≥0.9. (D) We compare the genome-wide distribution of Residual Variation Intolerance Score (RVIS) percentiles to those of genes affected by hcoErosion. By and large, hcoErosion genes are more tolerant of common functional variation in humans, suggesting that selection over coding genes is similar across mammalians. Several genes at the lower tail of the RVIS percentiles are highlighted (see Table 3 for details).

involve HGMD (28) genes implicated in severe human congenital disorders (Table 2, see Materials and Methods). Furthermore, three hcoErosion genes are pLI-predicted to be deleterious in human patients when mutated (Table 3, see Materials and Methods) (30). Using the Residual Variation Intolerance Score (RVIS) (29), which is a gene-based measure of intolerance to common genetic variation (with minor allele frequencies greater than 0.05%), we also found six genes predicted to be affected by hcoErosion that have an RVIS in the bottom quintile of all scored human genes (patients when mutated, see Materials and Methods).

Erosion of *GCKR* in microbats may facilitate their high-fat insectivorous diet

Microbats and megabats, the two primary suborders of bats, have vastly different diets. Microbats have extremely fat-rich, insect-based diets (42), while megabats have fruit-based diets depleted of fat (43). We found that *GCKR* (Glucokinase regulatory protein; OMIM: 600842), variants of which are associated with elevated high-density lipoprotein (HDL) cholestrol in human (44), is specifically eroded in microbats (see Figure 6 and Table 2). This potentially provides a genotypic basis for an observation by Widmaier et al. (45) who found that HDL-cholestrol levels in a lactating microbat species (*Tadarida brasiliensis mexicana*) were 10-fold higher in comparison to three species of megabats. Specifically, they proposed that these extraordinarily high HDL levels, possibly facilitated by *GCKR* erosion, could explain why microbats are protected from atherosclerosis and other common diseases associated with high-fat intake.

Erosion of *PKD1L1* and *MMP21* observed in artiodactyla (even-toed ungulates) but causes prenatal lethality in mice and congenital heart defects in humans

Pkd1l1 (polycystin kidney disease protein 1-like 1) null mutations in mice result in a high rate of embryonic lethal-

Table 1. Genes implicated in mammalian hcoErosions (high confidence ortholog erosions) that result in lethality when inactivated in mouse models

Gene	Mouse knockout phenotype	Species with gene hcoErosion
CA5B	Preweaning lethality, incomplete penetrance	Killer whale, dolphin
CCDC94	Embryonic lethality	Black flying-fox, megabat, microbat, big brown bat David's myotis bat
DMBT1	Embryonic lethality	^(I)^ Naked mole-rat, brush-tailed rat, guinea pig, chinchilla ^(II)^ Goat, sheep, Tibetan antelope, cow
HAP1	Lethality during fetal growth through weaning	Naked mole-rat, brush-tailed rat, guinea pig, chinchilla
MESP1	Embryonic lethality	Naked mole-rat, brush-tailed rat, guinea pig, chinchilla
MLKL	Embryonic lethality	Cat, dog, ferret, panda, pacific walrus, Weddell seal, horse, white rhinoceros
PKD1L1	Lethality throughout fetal growth and development	Alpaca, Bactrian camel, killer whale, dolphin, goat, sheep, Tibetan antelope, cow
RESP18	Prenatal lethality	Microbat, David's myotis bat
SERPINA10	Lethality, incomplete penetrance	^(I)^ Cat, dog, ferret, panda, pacific walrus, Weddell seal ^(II)^ Rabbit, pika
ZNF565	Embryonic lethality	Pacific walrus, Weddell seal

(I), (II) Independent hcoErosion loss events: (I) species belonging to group I (II) species belonging to group II.

ity (46) (Table 1) characterized by misregulated nodal signaling (47) and anomalous Left–Right (L–R) symmetry patterning (48,49) (Figure 7A). Indeed, humans with homozygous loss of function in *PKD1L1* (OMIM: 609721) present with laterality defects ranging from *Situs Inversus Totalis* to heterotaxy and with congenital heart disorders, all of which can be deleterious early in life (50). As such, it was remarkable to find *PKD1L1* hcoErosion, with deletion of as much as 98% of coding bases in some species, in a clade of nine even-toed ungulates (including cetaceans, see Figure 7B). Congruent with this finding, an Ensembl annotation for *PKD1L1* does not exist for the cow, sheep, dolphin, alpaca and pig genomes, and we detected no orthology between human *PKD1L1* to any other gene in these genomes. In contrast, we found high sequence homology for the human protein sequence of *PKD1L1* in the genomes of outgroup lineages such as horse and elephant, suggesting that the gene is intact in those species, and lost in artiodactyla (even-toed ungulates).

Interestingly, we also discovered a related hcoErosion in the same group of even-toed ungulates (including cetaceans) affecting the gene *MMP21* (Matrix Metalloproteinase 21; OMIM: 608416; Figure 7C) that encodes a component of Nodal signaling (50) and is also implicated in heterotaxy (51) and in congenital heart disorders (52,53) (Figure 7 A). Interestingly, Double Outlet Right Ventricle—a cardiac disorder associated with mutation in mouse *Mmp21* (54) and with mutation in human *PKD1L1* (50)—has significantly higher incidence in cattle with congenital heart disorder relative to human and other animals with this condition (55) (presumably because hcoErosion of *both PKD1L1* and *MMP21* naturally occurs in artiodactyla but not in other mammals).

Erosion of endocrine regulator *GPRC6A* evolved in odontoceti (toothed whales) but is associated with testicular insufficiency in humans and mice

GPRC6A (OMIM:613572) is a G protein-coupled receptor that plays an important role in metabolic and endocrine regulation (56). Highly expressed in Leydig cells of the testis (in addition to many other tissues), *GPRC6A* is activated by testosterone, osteocalcin, basic amino acids, and various cations (57,58). In mouse models, *Gprc6a* ablation results in dramatic decrease of testosterone levels, smaller testis size, and reduced sperm count (59). Similarly in humans, loss-of-function mutations in *GPRC6A* are associated with testicular insufficiency (subfertility, altered sperm parameters, low circulating testosterone levels, and high circulating luteinizing hormone levels) (60). A number of studies also found that *GPRC6A* is associated with prostate cancer progression and could serve as a potential drug target for this malignancy (58,61).

GPRC6A is a highly conserved gene across mammals and even has orthologs in species as distant as zebrafish (Figure 8), suggesting it may have arisen early in vertebrate evolution. It is highly remarkable then, that we observed hcoErosion of *GPRC6A* in dolphin and killer whale—where over 50% of amino acids are deleted in both species (including the entirety of exons 5 and 6), and the remaining regions contain several frameshift indels and nonsense mutations (Figure 8). The gene is well-conserved in outgroup bovidae (domestic goat, sheep, Tibetan antelope, and cow), suggesting it was functional in the cetartiodactyla ancestor (superorder of odontoceti and bovidae) but was inactivated and then allowed to erode in the evolutionary past of toothed whales. *GPRC6A* erosion in toothed whales is especially striking when considering that toothed whales exhibit 7–25 times greater testis-to-body mass ratio relative to other mammals (62). Alternatively, it is notable that *Gprc6a*-null mice also exhibit overall higher body fat percentage (59), which could offer a hypothesis for how blubber evolved in cetaceans.

DISCUSSION

In this work, we devised a novel approach to automate the survey of genomes for instances of coding gene sequence erosion. Knowledge of gene losses has far-reaching applications in studying the morphological and physiological adaptations of different species (10), in discovering alternative molecular pathways for critical genes (2), in medical genetics (13) and even in animal conservation programs (12). Our approach is both fully automated and includes steps

Table 2. Genes implicated in mammalian hcoErosions that harbor monogenic disease variants in human patients (disease mutations in HGMD (28))

Gene	Associated human monogenic disease	Species with gene hcoErosion
A2ML1	• Noonan syndrome • Otitis media (susceptibility to)	Naked mole-rat, brush-tailed rat, guinea pig, chinchilla
CETP	• Higher/Lower HDL cholesterol level • Hyperalphalipoproteinaemia • Cholesterol ester transfer protein deficiency	$^{(I)}$Bactrian camel, alpaca $^{(II)}$Goat, sheep, Tibetan antelope, cow
CRYBB3	• Cataract	Microbat, big brown bat, David's myotis bat
CRYGB	• Congenital cataract	Cape golden mole, tenrec
EYS	• Retinitis pigmentosa • Retinal dystrophy • Peripheral dystrophy • Usher syndrome	Mouse, rat, Chinese hamster, golden hamster, prairie vole
FCN2	• FCN2 deficiency	Goat, sheep, Tibetan antelope, cow
GCKR	• Elevated HDL-cholesterol • Hypertriglyceridaemia	Microbat, big brown bat, David's myotis bat
HMGCS2	• Mitochondrial HMG-CoA synthase deficiency	Black flying-fox, megabat
HSD3B2	• 3 beta-hydroxysteroid dehydrogenase deficiency • Adrenal hyperplasia • Hypospadias, non-syndromic • Idiopathic hypospadias • Pseudohermaphroditism	Goat, sheep, Tibetan antelope, cow
KLKB1	• Prekallikrein deficiency	Dolphin, killer whale
KRT3	• Corneal dystrophy, Meesmann	Mouse, rat
MESP1	• Tetralogy of Fallot • Ventricular septal defect	Naked mole-rat, brush-tailed rat, guinea pig, chinchilla
MMP21	• Heterotaxy	Pig, dolphin, killer whale, Bactrian camel, alpaca, goat, sheep, Tibetan antelope, cow
MYD88	• MYD88 deficiency	Brush-tailed rat, chinchilla
OPTC	• Glaucoma, primary open angle	Cape golden mole, tenrec, microbat, big brown bat, David's myotis bat
PCSK9	• Hypercholesterolaemia • Low/High LDL cholesterol	$^{(I)}$Cat, dog, ferret, panda, pacific walrus, Weddell seal $^{(II)}$Goat, sheep, Tibetan antelope, cow
PLA2G2A	• Colorectal cancer	Dolphin, killer whale
RIPPLY1	• Intellectual disability	Black flying-fox, megabat
SFXN4	• Colorectal cancer • Mitochondriopathy and macrocytic anaemia	$^{(I)}$Chinese hamster, golden hamster, prairie vole $^{(II)}$Naked mole-rat, brush-tailed rat, guinea pig, chinchilla
STAP1	• Hypercholesterolaemia	Dolphin, killer whale
TCN1	• Transcobalamin I deficiency	Mouse, rat
TNFRSF6B	• Systemic lupus erythematosus	Mouse, rat, Chinese hamster, golden hamster, prairie vole
UMOD	• Chronic kidney disease • Congenital anomalies of the kidney and urinary tract • FJHN/MCKD syndrome • Glomerulocystic kidney disease • Uromodulin-associated kidney disease • Hyperuricaemic nephropathy	Microbat, big brown bat, David's myotis bat, black flying-fox, megabat
XAF1	• Multiple sessile serrated adenoma	Cat, dog, ferret, panda, pacific walrus, Weddell seal
ZNF543	• IgA nephropathy	Cat, dog, ferret, panda, pacific walrus, Weddell seal
ZNF589	• Intellectual disability	Ferret, panda, pacific walrus, Weddell seal
ZP1	• Infertility	Pig, dolphin, killer whale, Bactrian camel, alpaca, goat, sheep, Tibetan antelope, cow

$^{(I), (II)}$ Independent hcoErosion loss events: $^{(I)}$ species belonging to group I $^{(II)}$ species belonging to group II.

to greatly minimize false positive predictions, which should appeal to downstream experimental predictions.

In particular, our conservative approach addresses a number of challenges that hindered previous attempts to automate screening. The two biggest potential confounders are mistaking paralogs for orthologs, and confusing sequencing assembly or alignment artifacts for real genomic changes. Our mapping procedure using whole-genome pairwise alignments is conservation of synteny-aware, is robust to sequencing gaps and other artifacts, and produces strictly one-to-one ortholog assignments that are not confounded by gene duplication events (paralogs) across species. Pairwise alignments for orthology mapping are more reliable than multi-sequence alignments (MSAs)—such as those generated by TBA/MULTIZ (63)—because, unlike MSAs, pairwise alignments help guarantee that the entire gene alignment maintains synteny and collinearity in both species and also allow us to ignore alignments where orthol-

Table 3. Mammalian hcoErosions that either have an RVIS (Residual Variation Intolerance Score) in the bottom quintile of all human genes analyzed and/or have a pLI (probability of being loss-of-function intolerant) score ≥ 0.9 (✓)

Gene	RVIS percentile	gnomAD pLI score ≥ 0.9	Species with hcoErosion
UBC	4.19%		(I) Hedgehog, Star-nosed mole, Shrew (II) Naked mole-rat, Guinea Pig, Chinchilla, Brush-tailed rat (III) Ferret, Panda, Pacific walrus, Weddell seal (IV) Alpaca, Bactrian camel
DDX60	6.02%		Tibetan antelope, Sheep, Domestic goat, Cow
PCDHA7	10.27%		Panda, Weddell seal, Ferret, Pacific walrus
ADAM30	10.78%	N/A	Guinea Pig, Brush-tailed rat, Naked mole-rat, Chinchilla
ZYG11B	14.34%	✓	Rhesus macaque, Crab-eating macaque
PPP2R2D	18.43%	✓	Tibetan antelope, Sheep, Domestic goat, Cow
DCAF12L1	22.73%	✓	Naked mole-rat, Guinea Pig, Chinchilla, Brush-tailed rat

(I), (II), (III), (IV) Independent hcoErosion loss events:
(I) species belonging to group I (II) species belonging to group II (III) species belonging to group III (IV) species belonging to group IV.

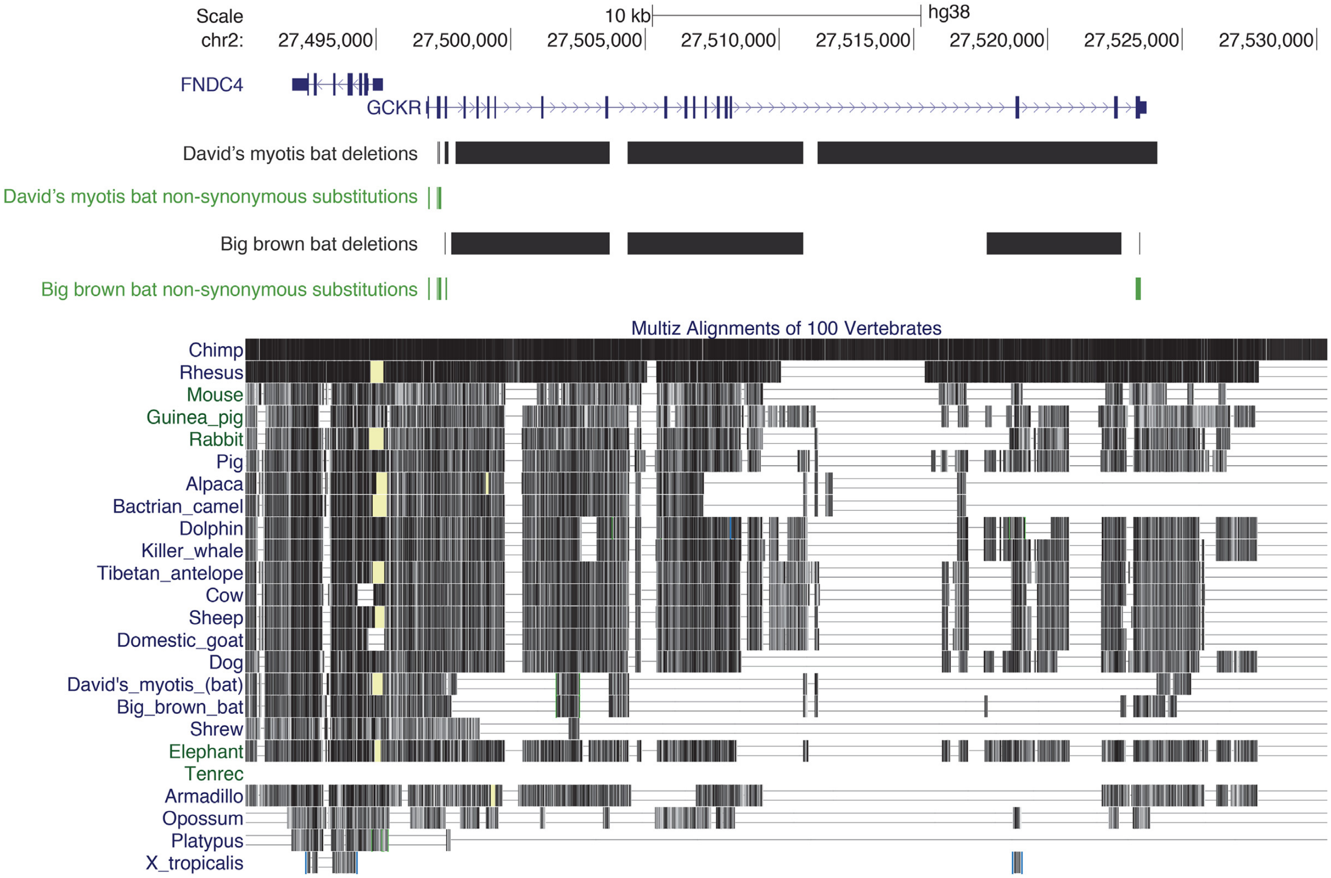

Figure 6. *GCKR* hcoErosion in microbats. A genome browser view of *GCKR* (Glucokinase regulatory protein) on the human genome (GRCh38) and a mammalian multiple alignment highlight coding lesions in microbat. Positions of deleted genomic fragments (black) and non-synonymous substitutions (green) are highlighted for David's myotis and big brown bat (both of *microchiroptera*). *GCKR* loss could explain why microbats are protected from common diseases associated with high-fat intake.

ogy cannot be determined with high confidence. To enrich for high-confidence gene erosion predictions, we used a Mahalanobis distance-based metric to refine the candidates to just those orthologs exhibiting extreme amounts of amino acid deletion and substitution relative to other genes in that species. To further minimize erroneous predictions, we distilled out just those candidates that are considered likely eroded in at least two closely related species but sequence-conserved in at least one other outgroup besides human.

Our method for detecting gene losses is, by design, necessarily conservative in order to maintain high accuracy and may not capture all gene loss events. For example, because our orthology mapping procedure (Figure 1) requires some portion of the reference gene to overlap at the query genome

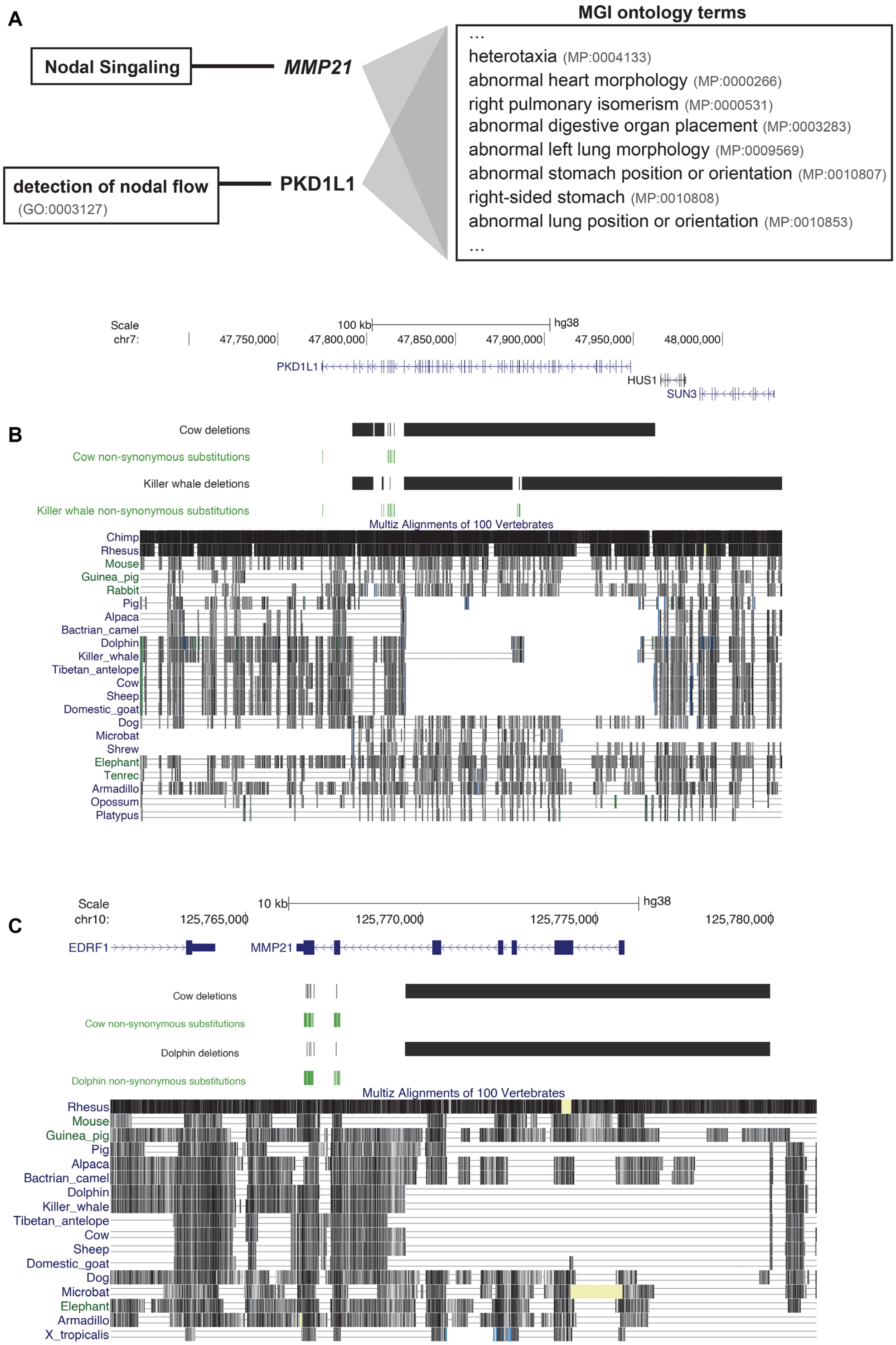

Figure 7. *PKD1L1* and *MMP21* hcoErosions in even-toed ungulates. (**A**) *PKD1L1* (Polycyctic kidney disease protein 1-like 1) and *MMP21* (Matrix Metalloproteinase 21) are both related to the Nodal signaling pathway, and null mutations in either gene results in severe laterality disorders with congenital heart defects. (**B**) A genome browser view of *PKD1L1* (on the human genome, GRCh38) and a mammalian multiple alignment highlight a clade-specific lesion of the gene in 9 even-toed ungulate species. Positions of deleted fragments (black) and non-synonymous substitutions (green) are highlighted for cow and killer whale. (**C**) *MMP21* has undergone hcoErosion in the same ancestor. Positions of deleted fragments (black) and non-synonymous substitutions (green) are highlighted for cow and dolphin. The morphological defect Double Outlet Right Ventricle has significantly higher incidence in cattle with congenital heart disorder relative to human and other animals with this condition (55) (perhaps because hcoErosion of both *PKD1L1* and *MMP21* naturally occurs in artiodactyla but not in other mammals).

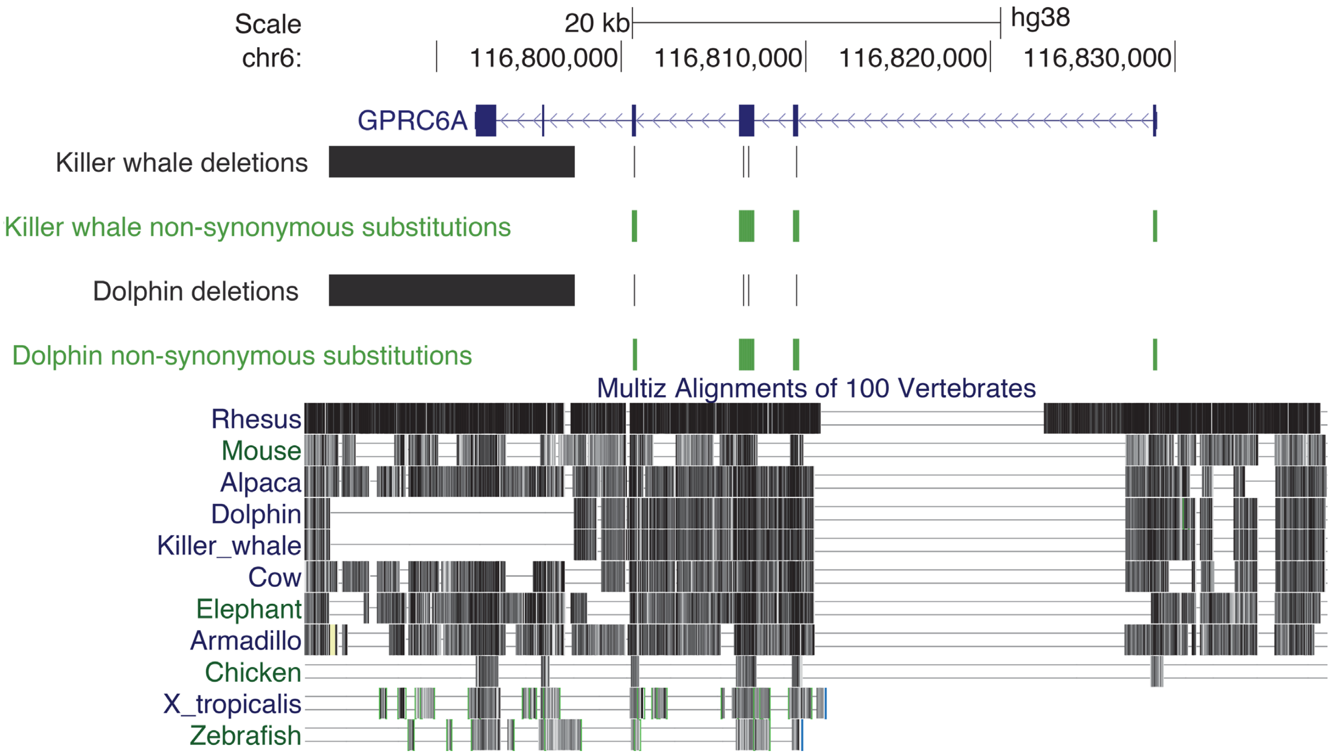

Figure 8. *GPRC6A* hcoErosion in toothed whales. A genome browser view of *GPRC6A* (on the human genome, GRCh38) and a mammalian multiple alignment highlight coding lesions in dolphin and killer whale. Positions of deleted fragments (black) and non-synonymous substitutions (green) are shown for both species. *GPRC6A* is a key hormonal and metabolic regulation protein, and the knockout of *GPRC6A* in male mice results in over 6-fold decrease of testosterone levels and reduced size and weight of the testis (59). Notably, toothed whales, like dolphin and killer whale, exhibit 7–25 times greater testis-to-body mass ratio relative to other mammals despite hcoErosion of *GPRC6A* (62).

locus where the gene loss has occurred, loss events that involved (i) complete deletion of the gene region; (ii) massive rearrangement disrupting conservation of synteny or (iii) sequence decay beyond what can be detected in the whole-genome alignment will not be identified as hcoErosions. Additionally, the phylogenetic filter discards all gene losses occurring only in a single species, some of which may well be fixed in this one species. Despite this conservative strategy, our method discovered 2192 hcoErosion events across 52 species (Supplementary Table S3).

Although the false positive rate (FPR) of our hcoErosion predictions is low (<10%, see Figure 4B), various factors can still contribute to its false positives. For instance, poor sensitivity of whole genome aligners can make entire gene exons appear to be missing (deleted) in a query species (64,65), particularly for genes with a high mutation rate, such as positively selected genes. Sensitive approaches to whole genome alignments have been shown to recover missing exons (66) and may help further reduce the already low FPR for hcoErosion predictions. We provide details on hcoErosion candidates which contradicted UniProt evidence (Supplementary Table S4) in order to facilitate future work investigating and minimizing the few remaining false positive results of our pipeline.

The evolutionary mechanisms contributing to these functionally significant gene losses were likely diverse. Some may have resulted from regressive evolution (i.e. degeneration of formerly useful anatomical and physiological functions), such as the degraded *OPTC* vision gene (67) in nocturnal microbats or the *CRYGB* erosion in subterranean cape golden moles (5). Other losses may have contributed to species adaptation, such as erosion of the epithelium gene *GSDMA* (68,69) in cetaceans which have skin adaptations to life in the water (10). Interestingly, we also found that skin-related terms were the most over-represented when we performed tissue and pathway enrichment analysis of our 412 unique hcoErosion genes (Supplementary Table S5 and Figure S2).

Species with hcoErosion that tolerate functional changes known to cause disease in humans provide intriguing potential for medical genetics (3,13). Some of these 'knockout experiments of nature' may tolerate and even derive selective advantage from gene loss(es) because of factors specific to their habitat niche. Others, however, may have evolved compensatory suppressor mutations to genetically negate otherwise deleterious consequences. It is these latter cases that could be harnessed for treating human congenital disorders (3,13). For instance, despite the erosion of *GPRC6A* in toothed whales, these magnificent creatures have relatively massive testes for their size—the categorically opposite phenotype for this gene when inactivated in mice and humans. We posit that further examination of odontoceti could reveal complementary testis development pathways that might inform therapy for male hypogonadism.

Extension of this gene loss survey to additional or newly sequenced species across the metazoan tree of life will likely reveal more such evolutionary curiosities with great clinical potential. To that end, we emphasize the ease with which genomes can be added to analyses using our approach. Each additional genome would independently be aligned to the reference assembly—without the high computational cost of realigning all genomes, as is necessary for methods requiring multiple-sequence alignments. Thus, our approach is easily scalable for the ever-increasing number of new species being sequenced (15,70).

DATA AVAILABILITY

The source code for the automated hcoErosions pipeline is available at http://bitbucket.org/bejerano/hcoerosions.

SUPPLEMENTARY DATA

Supplementary Data are available at NAR Online.

ACKNOWLEDGEMENTS

We thank members of the Bejerano Laboratory, particularly M.J. Berger, K. Jagadeesh, J. Birgmeier and B. Yoo, for technical advice and helpful discussions; Hiram Clawson and the UCSC Genome Browser team for providing the mammalian alignment chains, multiple sequence alignments and technical advice; Robin Jia for his contribution to the code for extracting coding sequences from alignment chains; D. Cooper and P. Stenson for Human Gene Mutation Database (HGMD) access; and Leigh Darryl Quarles for his insights into GPRC6A function.

FUNDING

H. I. Chen was funded in part by a National Science Foundation Graduate Research Fellowship Program [1656518] and by a National Institutes of Health Genetics and Developmental Biology Training Program [5T32GM007790]. G. Bejerano is funded by the National Human Genome Research Institute [R01HG008742]. Funding for open access charge: NIH [R01HG008742].

Conflict of interest statement. None declared.

REFERENCES

1. O'Leary,M.A. and Kaufman,S. (2011) MorphoBank: phylophenomics in the 'cloud'. *Cladistics*, **27**, 529–537.
2. Albalat,R. and Cañestro,C. (2016) Evolution by gene loss. *Nat. Rev. Genet.*, **17**, 379–391.
3. Hiller,M., Schaar,B.T., Indjeian,V.B., Kingsley,D.M., Hagey,L.R. and Bejerano,G. (2012) A 'forward genomics' approach links genotype to phenotype using independent phenotypic losses among related species. *Cell Rep.*, **2**, 817–823.
4. Marcovitz,A., Jia,R. and Bejerano,G. (2016) 'Reverse Genomics' Predicts Function of Human Conserved Noncoding Elements. *Mol. Biol. Evol.*, **33**, 1358–1369.
5. Partha,R., Chauhan,B.K., Ferreira,Z., Robinson,J.D., Lathrop,K., Nischal,K.K., Chikina,M. and Clark,N.L. (2017) Subterranean mammals show convergent regression in ocular genes and enhancers, along with adaptation to tunneling. *eLife*, **6**, e25884.
6. Emerling,C.A. and Springer,M.S. (2014) Eyes underground: regression of visual protein networks in subterranean mammals. *Mol. Phylogenet. Evol.*, **78**, 260–270.
7. Jiang,P., Josue,J., Li,X., Glaser,D., Li,W., Brand,J.G., Margolskee,R.F., Reed,D.R. and Beauchamp,G.K. (2012) Major taste loss in carnivorous mammals. *Proc. Natl. Acad. Sci. U.S.A.*, **109**, 4956–4961.
8. McGowen,M.R., Gatesy,J. and Wildman,D.E. (2014) Molecular evolution tracks macroevolutionary transitions in Cetacea. *Trends. Ecol. Evol.*, **29**, 336–346.
9. Strasser,B., Mlitz,V., Fischer,H., Tschachler,E. and Eckhart,L. (2015) Comparative genomics reveals conservation of filaggrin and loss of caspase-14 in dolphins. *Exp. Dermatol.*, **24**, 365–369.
10. Sharma,V., Hecker,N., Roscito,J.G., Foerster,L., Langer,B.E. and Hiller,M. (2018) A genomics approach reveals insights into the importance of gene losses for mammalian adaptations. *Nat. Commun.*, **9**, 1215.
11. Braun,B.A., Marcovitz,A., Camp,J.G., Jia,R. and Bejerano,G. (2015) Mx1 and Mx2 key antiviral proteins are surprisingly lost in toothed whales. *Proc. Natl. Acad. Sci. U.S.A.*, **112**, 8036–8040.
12. Meyer,W.K., Jamison,J., Richter,R., Woods,S.E., Partha,R., Kowalczyk,A., Kronk,C., Chikina,M., Bonde,R.K., Crocker,D.E. *et al.* (2018) Ancient convergent losses of Paraoxonase 1 yield potential risks for modern marine mammals. *Science*, **361**, 591–594.
13. Emerling,C.A., Widjaja,A.D., Nguyen,N.N. and Springer,M.S. (2017) Their loss is our gain: regressive evolution in vertebrates provides genomic models for uncovering human disease loci. *J. Med. Genet.*, **54**, 787–794.
14. Harrow,J., Denoeud,F., Frankish,A., Reymond,A., Chen,C.-K., Chrast,J., Lagarde,J., Gilbert,J.G., Storey,R., Swarbreck,D. *et al.* (2006) GENCODE: producing a reference annotation for ENCODE. *Genome Biol.*, **7**, S4.
15. of Scientists,G. K.C. (2009) Genome 10K: a proposal to obtain whole-genome sequence for 10 000 vertebrate species. *J. Hered.*, **100**, 659–674.
16. Huelsmann,M., Hecker,N., Springer,M.S., Gatesy,J., Sharma,V. and Hiller,M. (2019) Genes lost during the transition from land to water in cetaceans highlight genomic changes associated with aquatic adaptations. *Sci. Adv.*, **5**, eaaw6671.
17. Yates,A.D., Achuthan,P., Akanni,W., Allen,J., Allen,J., Alvarez-Jarreta,J., Amode,M.R., Armean,I.M., Azov,A.G., Bennett,R. *et al.* (2019) Ensembl 2020. *Nucleic Acids Res.*, **48**, D682–D688.
18. Bateman,A., Martin,M.J., O'Donovan,C., Magrane,M., Alpi,E., Antunes,R., Bely,B., Bingley,M., Bonilla,C., Britto,R. *et al.* (2017) UniProt: the universal protein knowledgebase. *Nucleic Acids Res.*, **45**, D158–D169.
19. Zhang,G., Li,C., Li,Q., Li,B., Larkin,D.M., Lee,C., Storz,J.F., Antunes,A., Greenwold,M.J., Meredith,R.W. *et al.* (2014) Comparative genomics reveals insights into avian genome evolution and adaptation. *Science*, **346**, 1311–1320.
20. Venkatesh,B. (2003) Evolution and diversity of fish genomes. *Curr. Opin. Genet. Dev.*, **13**, 588–592.
21. Clark,A.G., Eisen,M.B., Smith,D.R., Bergman,C.M., Oliver,B., Markow,T.A., Kaufman,T.C., Kellis,M., Gelbart,W., Iyer,V.N. *et al.* (2007) Evolution of genes and genomes on the Drosophila phylogeny. *Nature*, **450**, 203–218.
22. Kent,W.J., Baertsch,R., Hinrichs,A., Miller,W. and Haussler,D. (2003) Evolution's cauldron: Duplication, deletion, and rearrangement in the mouse and human genomes. *Proc. Natl. Acad. Sci. U.S.A.*, **100**, 11484–11489.
23. Marcovitz,A., Turakhia,Y., Chen,H.I., Gloudemans,M., Braun,B.A., Wang,H. and Bejerano,G. (2019) A functional enrichment test for molecular convergent evolution finds a clear protein-coding signal in echolocating bats and whales. *Proc. Natl. Acad. Sci. U.S.A.*, **116**, 21094–21103.
24. Mahalanobis,P.C. (1936) In: *On the Generalized Distance in Statistics*. National Institute of Science of India.
25. De Maesschalck,R., Jouan-Rimbaud,D. and Massart,D.L. (2000) The mahalanobis distance. *Chemometr. Intell. Lab.*, **50**, 1–18.
26. Kent,W.J. (2002) BLAT the BLAST-like alignment tool. *Genome Res.*, **12**, 656–664.
27. Dickinson,M.E., Flenniken,A.M., Ji,X., Teboul,L., Wong,M.D., White,J.K., Meehan,T.F., Weninger,W.J., Westerberg,H., Adissu,H. *et al.* (2016) High-throughput discovery of novel developmental phenotypes. *Nature*, **537**, 508–514.

28. Stenson,P.D., Mort,M., Ball,E.V., Evans,K., Hayden,M., Heywood,S., Hussain,M., Phillips,A.D. and Cooper,D.N. (2017) The Human Gene Mutation Database: towards a comprehensive repository of inherited mutation data for medical research, genetic diagnosis and next-generation sequencing studies. *Hum. Genet.*, **136**, 665–677.
29. Petrovski,S., Gussow,A.B., Wang,Q., Halvorsen,M., Han,Y., Weir,W.H., Allen,A.S. and Goldstein,D.B. (2015) The intolerance of regulatory sequence to genetic variation predicts gene dosage sensitivity. *PLOS Genet.*, **11**, e1005492.
30. Lek,M., Karczewski,K.J., Minikel,E.V., Samocha,K.E., Banks,E., Fennell,T., O'Donnell-Luria,A.H., Ware,J.S., Hill,A.J., Cummings,B.B. *et al.* (2016) Analysis of protein-coding genetic variation in 60,706 humans. *Nature*, **536**, 285–291.
31. Rivals,I., Personnaz,L., Taing,L. and Potier,M.-C. (2006) Enrichment or depletion of a GO category within a class of genes: which test? *Bioinformatics*, **23**, 401–407.
32. Jain,A. and Tuteja,G. (2019) TissueEnrich: tissue-specific gene enrichment analysis. *Bioinformatics*, **35**, 1966–1967.
33. McLean,C.Y., Bristor,D., Hiller,M., Clarke,S.L., Schaar,B.T., Lowe,C.B., Wenger,A.M. and Bejerano,G. (2010) GREAT improves functional interpretation of cis-regulatory regions. *Nat. Biotechnol.*, **28**, 495.
34. Derrien,T., Thézé,J., Vaysse,A., André,C., Ostrander,E.A., Galibert,F. and Hitte,C. (2009) Revisiting the missing protein-coding gene catalog of the domestic dog. *BMC genomics*, **10**, 62.
35. Hogarth,C.A., Roy,A. and Ebert,D.L. (2003) Genomic evidence for the absence of a functional cholesteryl ester transfer protein gene in mice and rats. *Comp. Biochem. Phys. B*, **135**, 219–229.
36. Abd El-Aziz,M.M., Barragan,I., O'Driscoll,C.A., Goodstadt,L., Prigmore,E., Borrego,S., Mena,M., Pieras,J.I., El-Ashry,M.F., Safieh,L.A. *et al.* (2008) EYS, encoding an ortholog of Drosophila spacemaker, is mutated in autosomal recessive retinitis pigmentosa. *Nat. Genet.*, **40**, 1285–1287.
37. Bowling,S., Di Gregorio,A., Sancho,M., Pozzi,S., Aarts,M., Signore,M., D Schneider,M., Barbera,J.P.M., Gil,J. and Rodríguez,T.A. (2018) P53 and mTOR signalling determine fitness selection through cell competition during early mouse embryonic development. *Nat. Commun.*, **9**, 1763.
38. Su,R.-W., Strug,M.R., Jeong,J.-W., Miele,L. and Fazleabas,A.T. (2016) Aberrant activation of canonical Notch1 signaling in the mouse uterus decreases progesterone receptor by hypermethylation and leads to infertility. *Proc. Natl. Acad. Sci. U.S.A.*, **113**, 2300–2305.
39. Hargrave,M., Wright,E., Kun,J., Emery,J., Cooper,L. and Koopman,P. (1997) Expression of the Sox11 gene in mouse embryos suggests roles in neuronal maturation and epithelio-mesenchymal induction. *Dev. Dyn.*, **210**, 79–86.
40. Greibe,E., Fedosov,S. and Nexo,E. (2012) The cobalamin-binding protein in zebrafish is an intermediate between the three cobalamin-binding proteins in human. *PLoS One*, **7**, e35660.
41. Goudet,G., Mugnier,S., Callebaut,I. and Monget,P. (2008) Phylogenetic analysis and identification of pseudogenes reveal a progressive loss of zona pellucida genes during evolution of vertebrates. *Biol. Reprod.*, **78**, 796–806.
42. Phillips,C.J., Phillips,C.D., Goecks,J., Lessa,E.P., Sotero-Caio,C.G., Tandler,B., Gannon,M.R. and Baker,R.J. (2014) Dietary and flight energetic adaptations in a salivary gland transcriptome of an insectivorous bat. *PLoS One*, **9**, e83512.
43. Voigt,C.C., Zubaid,A., Kunz,T.H. and Kingston,T. (2011) Sources of assimilated proteins in Old and New World phytophagous bats. *Biotropica*, **43**, 108–113.
44. Singaraja,R.R., Tietjen,I., Hovingh,G.K., Franchini,P.L., Radomski,C., Wong,K., Stylianou,I.M., Lin,L., Wang,L., Mitnaul,L. *et al.* (2014) Identification of four novel genes contributing to familial elevated plasma HDL cholesterol in humans. *J. lipid Res.*, **55**, 1693–1701.
45. Widmaier,E., Gornstein,E., Hennessey,J., Bloss,J., Greenberg,J. and Kunz,T. (1996) High plasma cholesterol, but low triglycerides and plaque-free arteries, in Mexican free-tailed bats. *Am. J. Physiol.-Reg. I*, **271**, R1101–R1106.
46. Vogel,P., Read,R., Hansen,G.M., Freay,L.C., Zambrowicz,B.P. and Sands,A.T. (2010) Situs inversus in Dpcd/Poll-/-, Nme7-/- , and Pkd1l1-/- mice. *Vet. Pathol.*, **47**, 120–131.
47. Field,S., Riley,K.-L., Grimes,D.T., Hilton,H., Simon,M., Powles-Glover,N., Siggers,P., Bogani,D., Greenfield,A. and Norris,D.P. (2011) Pkd1l1 establishes left-right asymmetry and physically interacts with Pkd2. *Development*, **138**, 1131–1142.
48. Grimes,D.T., Keynton,J.L., Buenavista,M.T., Jin,X., Patel,S.H., Kyosuke,S., Vibert,J., Williams,D.J., Hamada,H., Hussain,R. *et al.* (2016) Genetic analysis reveals a hierarchy of interactions between polycystin-encoding genes and genes controlling cilia function during left-right determination. *PLoS Genet.*, **12**, e1006070.
49. Kamura,K., Kobayashi,D., Uehara,Y., Koshida,S., Iijima,N., Kudo,A., Yokoyama,T. and Takeda,H. (2011) Pkd1l1 complexes with Pkd2 on motile cilia and functions to establish the left-right axis. *Development*, **138**, 1121–1129.
50. Vetrini,F., DâĂŹAlessandro,L.C.A., Akdemir,Z.C., Braxton,A., Azamian,M.S., Eldomery,M.K., Miller,K., Kois,C., Sack,V., Shur,N. *et al.* (2016) Bi-allelic mutations in PKD1L1 are associated with laterality defects in humans. *Am. J. Hum. Genet.*, **99**, 886–893.
51. Perles,Z., Moon,S., Ta-Shma,A., Yaacov,B., Francescatto,L., Edvardson,S., Rein,A. J. J.T., Elpeleg,O. and Katsanis,N. (2015) A human laterality disorder caused by a homozygous deleterious mutation in MMP21. *J. Med. Genet.*, **52**, 840–847.
52. Akawi,N., McRae,J., Ansari,M., Balasubramanian,M., Blyth,M., Brady,A.F., Clayton,S., Cole,T., Deshpande,C., Fitzgerald,T.W. *et al.* (2015) Discovery of four recessive developmental disorders using probabilistic genotype and phenotype matching among 4,125 families. *Nat. Genet.*, **47**, 1363–1369.
53. Li,Y., Klena,N.T., Gabriel,G.C., Liu,X., Kim,A.J., Lemke,K., Chen,Y., Chatterjee,B., Devine,W., Damerla,R.R. *et al.* (2015) Global genetic analysis in mice unveils central role for cilia in congenital heart disease. *Nature*, **521**, 520–524.
54. Eppig,J.T., Smith,C.L., Blake,J.A., Ringwald,M., Kadin,J.A., Richardson,J.E. and Bult,C.J. (2017) Mouse genome informatics (MGI): resources for mining mouse genetic, genomic, and biological data in support of primary and translational research. *Methods Mol. Biol.*, **1488**, 47–73.
55. Michaëlsson,M. and Ho,S.Y. (2000) In: *Congenital Heart Malformations in Mammals: An Illustrated Text*. Imperial Collage Press, London, UK.
56. Clemmensen,C., Smajilovic,S., Wellendorph,P. and Bräuner-Osborne,H. (2014) The GPCR, class C, group 6, subtype A (GPRC6A) receptor: from cloning to physiological function. *Brit. J. Pharmacol.*, **171**, 1129–1141.
57. Pi,M. and Quarles,L.D. (2012) Multiligand specificity and wide tissue expression of GPRC6A reveals new endocrine networks. *Endocrinology*, **153**, 2062–2069.
58. Pi,M. and Quarles,L.D. (2012) GPRC6A regulates prostate cancer progression. *Prostate*, **72**, 399–409.
59. Pi,M., Chen,L., Huang,M.-Z., Zhu,W., Ringhofer,B., Luo,J., Christenson,L., Li,B., Zhang,J., Jackson,P.D. *et al.* (2008) GPRC6A null mice exhibit osteopenia, feminization and metabolic syndrome. *PLoS ONE*, **3**, e3858.
60. De Toni,L., Di Nisio,A., Speltra,E., Rocca,M.S., Ghezzi,M., Zuccarello,D., Turiaco,N., Ferlin,A. and Foresta,C. (2016) Polymorphism rs2274911 of GPRC6A as a Novel Risk Factor for Testis Failure. *J. Clin. Endocr. Metab.*, **101**, 953–961.
61. Ye,R., Pi,M., Cox,J.V., Nishimoto,S.K. and Quarles,L.D. (2017) CRISPR/Cas9 targeting of GPRC6A suppresses prostate cancer tumorigenesis in a human xenograft model. *J. Exp. Clin. Canc. Res.: CR*, **36**, 90 .
62. Kenagy,G.J. and Trombulak,S.C. (1986) Size and function of mammalian testes in relation to body size. *J. Mammal.*, **67**, 1–22.
63. Blanchette,M., Kent,W.J., Riemer,C., Elnitski,L., Smit,A.F., Roskin,K.M., Baertsch,R., Rosenbloom,K., Clawson,H., Green,E.D. *et al.* (2004) Aligning multiple genomic sequences with the threaded blockset aligner. *Genome Res.*, **14**, 708–715.
64. McLean,C.Y., Reno,P.L., Pollen,A.A., Bassan,A.I., Capellini,T.D., Guenther,C., Indjeian,V.B., Lim,X., Menke,D.B., Schaar,B.T. *et al.* (2011) Human-specific loss of regulatory DNA and the evolution of human-specific traits. *Nature*, **471**, 216–219.
65. Sharma,V. and Hiller,M. (2017) Increased alignment sensitivity improves the usage of genome alignments for comparative gene annotation. *Nucleic Acids Res.*, **45**, 8369–8377.
66. Turakhia,Y., Goenka,S.D., Bejerano,G. and Dally,W.J. (2019) Darwin-WGA: A co-processor provides increased sensitivity in whole

genome alignments with high speedup. In: *2019 IEEE International Symposium on High Performance Computer Architecture (HPCA)*, IEEE, pp. 359–372.

67. Acharya,M., Mookherjee,S., Bhattacharjee,A., Thakur,S. K.D., Bandyopadhyay,A.K., Sen,A., Chakrabarti,S. and Ray,K. (2007) Evaluation of the OPTC gene in primary open angle glaucoma: functional significance of a silent change. *BMC Mol. Biol.*, **8**, 21.
68. Saeki,N., Kuwahara,Y., Sasaki,H., Satoh,H. and Shiroishi,T. (2000) Gasdermin (Gsdm) localizing to mouse Chromosome 11 is predominantly expressed in upper gastrointestinal tract but significantly suppressed in human gastric cancer cells. *Mamm. Genome*, **11**, 718–724.
69. Saeki,N., Kim,D.H., Usui,T., Aoyagi,K., Tatsuta,T., Aoki,K., Yanagihara,K., Tamura,M., Mizushima,H., Sakamoto,H. *et al.* (2007) GASDERMIN, suppressed frequently in gastric cancer, is a target of LMO1 in TGF-beta-dependent apoptotic signalling. *Oncogene*, **26**, 6488–6498.
70. Lewin,H.A., Robinson,G.E., Kress,W.J., Baker,W.J., Coddington,J., Crandall,K.A., Durbin,R., Edwards,S.V., Forest,F., Gilbert,M.T.P. *et al.* (2018) Earth BioGenome project: sequencing life for the future of life. *Proc. Natl. Acad. Sci. U.S.A.*, **115**, 4325–4333.